PLANETARY SCIENCE

Transient HCl in the atmosphere of Mars

Oleg Korablev[1]*, Kevin S. Olsen[2], Alexander Trokhimovskiy[1], Franck Lefèvre[3], Franck Montmessin[3], Anna A. Fedorova[1], Michael J. Toplis[4], Juan Alday[2], Denis A. Belyaev[1], Andrey Patrakeev[1], Nikolay I. Ignatiev[1], Alexey V. Shakun[1], Alexey V. Grigoriev[1], Lucio Baggio[3], Irbah Abdenour[3], Gaetan Lacombe[3], Yury S. Ivanov[5], Shohei Aoki[6,7], Ian R. Thomas[7], Frank Daerden[7], Bojan Ristic[7], Justin T. Erwin[7], Manish Patel[8], Giancarlo Bellucci[9], Jose-Juan Lopez-Moreno[10], Ann C. Vandaele[7]

A major quest in Mars' exploration has been the hunt for atmospheric gases, potentially unveiling ongoing activity of geophysical or biological origin. Here, we report the first detection of a halogen gas, HCl, which could, in theory, originate from contemporary volcanic degassing or chlorine released from gas-solid reactions. Our detections made at ~3.2 to 3.8 μm with the Atmospheric Chemistry Suite and confirmed with Nadir and Occultation for Mars Discovery instruments onboard the ExoMars Trace Gas Orbiter, reveal widely distributed HCl in the 1- to 4-ppbv range, 20 times greater than previously reported upper limits. HCl increased during the 2018 global dust storm and declined soon after its end, pointing to the exchange between the dust and the atmosphere. Understanding the origin and variability of HCl shall constitute a major advance in our appraisal of martian geo- and photochemistry.

INTRODUCTION

Chlorine is present in the atmospheres of Earth and Venus and plays a critical role in their photochemical cycles. In Earth's troposphere, hydrogen chloride (HCl) is mainly sourced from sea salt aerosols, and its abundance partly controls the oxidizing potential of the atmosphere by interacting with ozone and hydroxyl radicals (OH) (*1*). In the stratosphere, relatively inert HCl is the main reservoir species, releasing chlorine radicals in heterogeneous processes that subsequently participate in ozone layer chemistry and seasonal polar ozone depletion. On Venus, HCl is also the dominant reservoir of chlorine, and its destruction via photolysis produces reactive chlorine species that are critical to the stability of its CO_2 atmosphere (*2*). HCl has never been observed in the atmosphere of Mars but has been suggested and sought as an indicator of active magmatic processes (*3*). Stringent upper limits of 0.2 to 0.3 parts per billion volume (ppbv) were established (*4*, *5*).

The primary science goal of the European Space Agency (ESA)–Roscosmos ExoMars Trace Gas Orbiter (TGO) mission is to make highly sensitive measurements of trace atmospheric species, including volcanic gases (*6*). TGO carries two dedicated spectrometers, the Atmospheric Chemistry Suite (ACS) (*7*) and the Nadir and Occultation for Mars Discovery (NOMAD) suite (*8*). From the start of the mission in April 2018, the TGO instruments measured multiple known atmospheric gases and their isotopologues (*9*–*15*).

RESULTS

Here, we discuss the first positive detection of a previously undetected gas-phase molecule in the atmosphere of Mars by TGO, hydrogen chloride (HCl). Figure 1 shows a sequence of spectra that highlight the HCl absorption features detected by ACS. They were measured on 4 January 2019 at 73°S latitude [heliocentric solar longitude (L_S) = 318°, late northern winter or southern summer on Mars]. As the instrument's line of sight (LOS) moves deeper into the atmosphere during a solar occultation (SO) (*7*), we can retrieve the vertical profile of the HCl mixing ratio (see Materials and Methods). The spectra are zoomed on the spectral ranges around three distinct features in the *R* branch of the HCl 1←0 transition band. The depth of absorption due to HCl reaches 3 to 4%, while the signal-to-noise ratio per pixel of the instrument, although dependent on the dust content in the atmosphere, is generally over 3000 to 5000. Neighboring absorption lines in Fig. 1 are caused by water, semiheavy water (HDO), and the $H^{37}Cl$ isotopologue of HCl. In all, ACS detects 12 spectral features belonging to $H^{35}Cl$ and $H^{37}Cl$ in the *P* and *R* branches of its ν_1 fundamental rotational band.

Figure S1 shows the wider spectral range covered by ACS and the contributions of different gases, and fig. S2 shows fits for HCl lines not shown in Fig. 1. The detection of HCl by ACS is corroborated by NOMAD measurements. HCl can be detected using several diffraction orders covering the 2600 to 3100 cm^{-1} spectral range (see fig. S3). The vertical profiles of the HCl mixing ratio are presented in Fig. 2. We observe three families of altitude profiles. In the Northern Hemisphere, mixing ratios of 1 to 2 ppbv are observed mostly at altitudes in the range of 15 to 25 km, decreasing toward the surface (Fig. 2A). In the Southern Hemisphere, a series of observations were made prior to L_S = 300°, during which time we were unable to probe below 15 km, but observed 2 to 3 ppbv between 20 and 30 km (Fig. 2B). After L_S = 300°, we observed higher abundances, but HCl was entirely constrained below 15 km (Fig. 2C). The differences between Fig. 2 (B and C) reflect changes in the physical state of the atmosphere as the dust storm declines, which are also tracked by water vapor and aerosols. During this time, dust settled to the surface and lower atmosphere, followed by cooling and contraction, and a lowering of the hygropause.

A latitudinal map of all HCl detections and upper limits is shown in Fig. 3A as a function of time, from L_S = 163° in Mars Year 34 (MY34) (April 2018) to L_S = 166° in MY35 (March 2020). For observations

[1]Space Research Institute (IKI), Moscow, Russia. [2]Department of Physics, University of Oxford, Oxford, UK. [3]Laboratoire Atmosphères, Milieux, Observations Spatiales (LATMOS/CNRS), Paris, France. [4]L'Institut de Recherche en Astrophysique et Planétologie (IRAP/CNRS), Toulouse, France. [5]Main Astronomical Observatory (MAO NASU), Kyiv, Ukraine. [6]LPAP, STAR Institute, Université de Liège, Liège, Belgium. [7]Royal Belgian Institute of Space Aeronomy (BIRA-IASB), Brussels, Belgium. [8]Open University, Milton-Keynes, UK. [9]Istituto di Astrofisica e Planetologia Spaziali (IAPS-INAF), Rome, Italy. [10]Instituto de Astrofisica de Andalucía (IAA/CSIC), Granada, Spain.
*Corresponding author. Email: korab@iki.rssi.ru

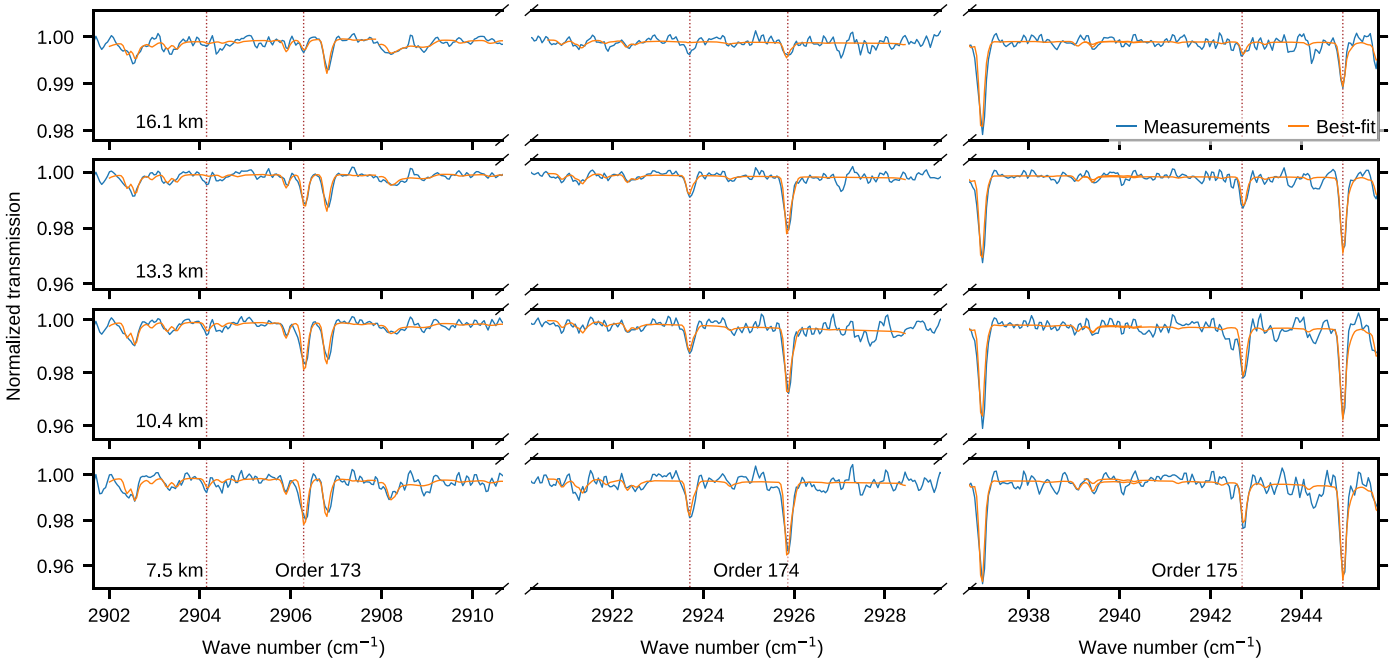

Fig. 1. Spectra and fits for windows in orders 173 to 175 containing the first ($H^{35}Cl$) and second ($H^{37}Cl$) isotopologues of HCl (line positions indicated with dashed vertical lines). Each panel shows spectra recorded as sequential tangent heights, indicating how the HCl features evolve with altitude. The occultation shown was recorded on L_S = 318° at a latitude −73.5°.

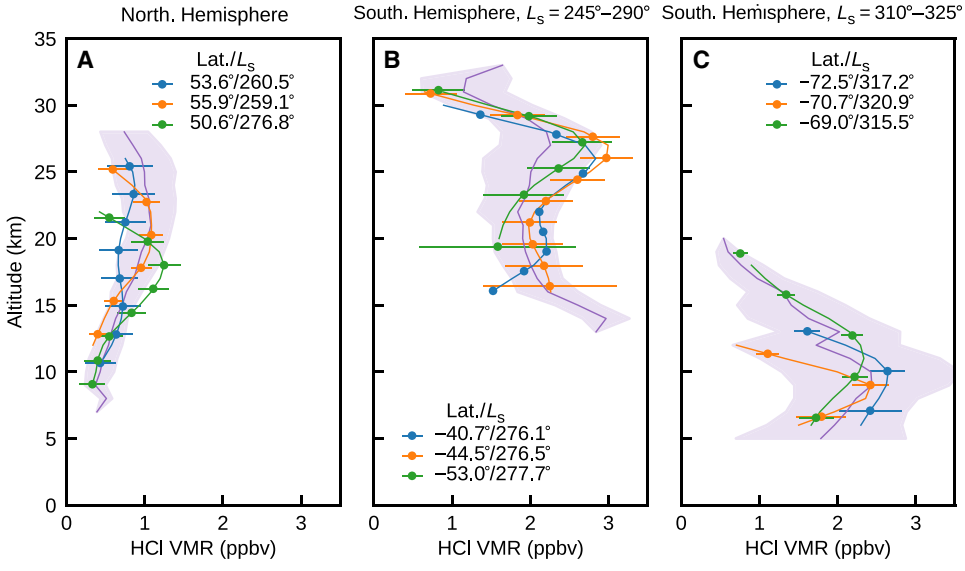

Fig. 2. Example HCl volume mixing ratio (VMR) vertical profiles retrieved from ACS MIR SO measurements. Profiles are grouped as (**A**) Northern Hemisphere observations between L_S = 210° and 330°, (**B**) Southern Hemisphere observations between L_S = 245° to 290°, and (**C**) Southern Hemisphere observation between L_S = 310° and 325°. Retrievals on a 1-km grid are shown as solid lines, and retrievals at the tangent heights are shown at points with uncertainties derived from the retrievals matrix of partial derivatives. The mean of the ensemble is shown in purple with a shaded area showing the SD. The ensemble of retrievals is shown in fig. S4.

where HCl is not observed, a lower limit is given (see fig. S5), which is generally <0.2 ppbv and often ~0.1 ppbv. No firm detection was made between the beginning of the TGO science phase until the global dust storm (GDS) period. A few values have been retrieved with a 1-sigma confidence level, but they have the same magnitude (<1 ppbv) as the upper limits established in nearby occultations and those previously set by ground-based observations of 0.3 to 0.6 ppbv (*4*, *5*). HCl is detected starting from L_S = 230° and persists until around L_S = 350°. There are over 140 positive detections made by ACS and nearly 50 by NOMAD over the same time period.

This time period, coinciding with seasonally enhanced dust, was punctuated by the onset of a GDS, beginning in the Southern Hemisphere around L_S = 190°, followed by a second, regional, storm at around L_S = 320°, with dust persisting through L_S = 190° to 350° (*16*).

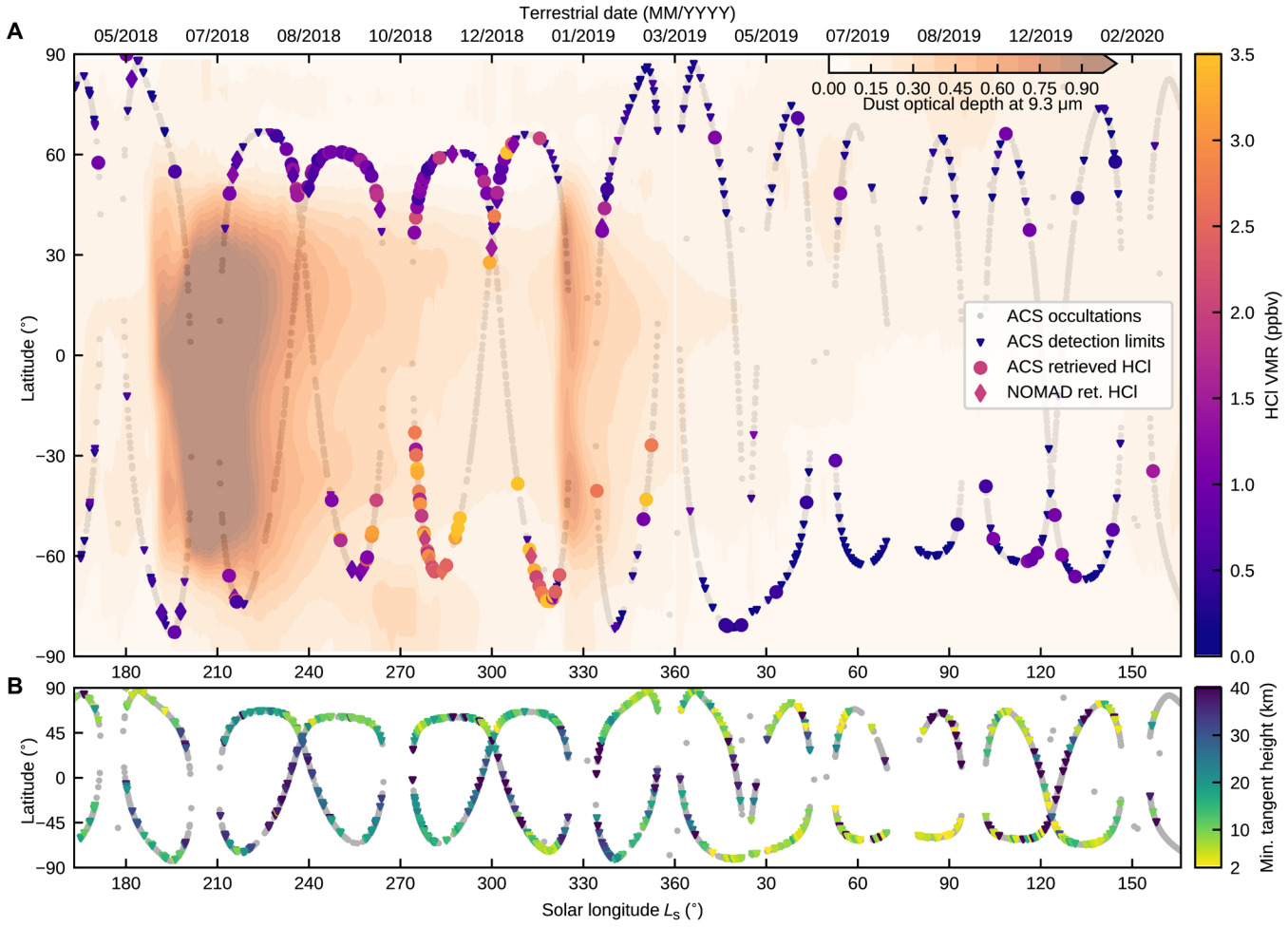

Fig. 3. Locations of ACS MIR occultations over time (L_s) and latitude. All ACS MIR occultations are shown in gray, and those with the spectral range used for HCl, but not bearing strong HCl signatures, are shown as triangles, with the color indicating a lower limit of the HCl VMR. Observations with detected HCl lines are indicated with circles and colored by their maximum retrieved HCl mixing ratio at between 10 and 30 km. Additional retrievals using NOMAD SO are shown with diamonds. Science operations began on $L_S = 163°$ in MY34 and continued through $L_S = 166°$ in MY35 at the time of writing. The GDS commenced around 190° and was followed by a second storm around $L_S = 320°$, and the mean dust opacity (*16*) is shown in (**A**). (**B**) The corresponding lowest usable tangent height for ACS observations, limited by transmission levels below this point being only a few percent.

The dust, lofted to heights of 30 to 50 km, is radiatively active and causes the atmosphere to heat and expand while intensifying Hadley cell circulation. Water vapor normally restricted to near the surface is elevated to create a hygropause near 80 km with mixing ratios around 150 ppmv, as observed by TGO (*11*, *12*) and reproduced by modeling (*17*). Dust affects SO observations in such a way that the dust storm imposed limits on the lowest observable altitude of TGO instruments. Figure 3B shows the corresponding minimum altitude in the atmosphere that we can observe due to aerosol loading (see also fig. S6). Still, even during the peak of the GDS, polar latitudes remained relatively free from aerosols. During this period, we begin to see HCl frequently in the Northern and Southern Hemispheres, suggesting HCl was already present and spread by atmospheric circulation. During the decline of the storm (from L_S ~ 240°) and through the whole perihelion season, the map shows the densest, quasi-complete presence of HCl in both hemispheres, including a few detections at mid-latitudes, where observation conditions are not optimal. After the second regional dust storm of MY34, the detections become less frequent, and during MY35, we only occasionally see low levels of HCl in our spectra. At $L_S = 75°$, the HCl upper limit of ~0.1 ppbv that we derive from ACS is consistent with the upper limit of 0.3 ppbv (3-sigma) previously determined at the same season from the Herschel satellite (*4*).

DISCUSSION

The observations just described suggest that the source of HCl is aerosol chemistry occurring with the dust particles lofted into the atmosphere. However, this is not the only possible source of HCl, and the distributions observed by TGO may result from several possible interactions that may be interrelated. We must also emphasize that the geometry of the SO technique does not always allow us to observe the lowest few kilometers of the atmosphere that may also contain HCl, while previous searches for HCl observed the full atmospheric column and were sensitive to these layers.

An alternative explanation for the presence of HCl in the martian atmosphere is as a result of recent surface volcanism or subsurface magmatic activity. HCl is a minor gas emitted by terrestrial

volcanism, and past martian volcanism has been suggested to be the source of contemporary surface chloride minerals (*18*). However, we note that outgassing of HCl related to magmatism (whether directly at the surface or at depth) should be accompanied by seismic activity and a suite of other sulfur-bearing and carbon-bearing molecules. Such molecules, SO_2 in particular, have not been detected on Mars so far (*19*), and no correlation of HCl observations with Marsquakes measured by the InSight lander is apparent [noting that InSight measurements began at the end of February 2019 (L_S = 340°) and that seismicity on Mars is lower than projected (*20*)]. In addition, the fact that the HCl increase is detected almost simultaneously at very distant locations of both hemispheres is difficult to reconcile with local release at the surface.

In the terrestrial troposphere, the majority of the HCl is not volcanic but produced from reactions between acids and hydrated NaCl originating from sea-salt aerosols (*21*). While there are no marine aerosols currently produced on Mars, there is a notable coincidence between HCl detections made here and the particularly strong GDS of MY34. This suggests that physical or chemical processes in martian dust storms may trigger the release of reactive gas-phase chlorine from the material that constitutes the airborne dust. Chlorine is widespread at the surface (*22*), and in the martian dust, at levels reaching 1 % by weight (*23*). This chlorine may be present as halite (NaCl), a mineral observed in nakhlite meteorites that originated from Mars (*24*) and proposed to be the dominant form of chloride on the martian surface in certain areas observed from orbit (*25*). Alternatively, perchlorate (ClO^-_4) has been observed on the martian surface at high and low latitudes (*26*, *27*) and should be widely distributed (*28*). During a dust storm event, both of these forms of Cl may be lofted into the atmosphere, making chlorine readily available in the lower atmosphere at this time. Releasing gas-phase chlorine from chloride salts may involve hydration of the chlorine salts, which has been shown to be effective in martian conditions (*29*). This can be followed by oxidation reactions and the release of radicals. The latter mechanism remains speculative at martian conditions but would ultimately lead to the formation of HCl (*30*).

In detail, four different pathways can be considered: (i) As the GDSs, and that of 2018 in particular, are characterized by large H_2O mixing ratios up to very high altitudes (*11*, *12*, *31*), unusually strong concentrations of oxidants such as OH and HO_2 should be expected in the atmosphere. In this case, particularly efficient gas-surface oxidation processing of the dust aerosols during the GDS may release reactive chlorine, as is the case on Earth (*1*, *30*). This scenario is supported by a strong correlation between the observed HCl and H_2O profiles (see fig. S7). A simultaneous observation of elevated HCl, H_2O, and aerosols, which are governed by the same advection pattern, does not constitute direct evidence of a cause-and-effect relation between them. However, the detection of a sudden appearance of HCl only in the presence of dust (furthermore during unfavorable viewing conditions caused by the dust-rich environment) provides strong indirect support for this hypothesis.

(ii) Chlorine would be more efficiently released from dust via acidic oxidation, analogous to terrestrial processes. The availability of necessary acids in the martian atmosphere remains unknown, but photochemical modeling studies (*32*, *33*) have demonstrated that the presence of nitrates, identified on the martian surface (*34*) and a likely component of dust, should enable the production of acids, nitric acid (HNO_3), and peroxynitric acid (HNO_4). They oxidize dry chloride salts to make Cl_2 gas, which would rapidly photolyze to generate chlorine radicals (*35*), which then react with HO_2 (primarily) to form HCl.

(iii) Because of strong saltation processes, the GDS can mobilize dust grains that have not been previously exposed to UV light for long periods. Being lifted to high altitudes, chlorine-bearing molecules at the surface of airborne dust may break up under the effect of UV irradiation into gas-phase compounds, including chlorine. The potential to oxidize mineral chlorides by the action of UV radiation has been demonstrated in the laboratory (*36*), but more experimental work is required to determine the abundance of chloride radicals that could be released to the gas phase by such processes.

(iv) Chlorine could be released by the volatilization of chloride minerals by electrical discharges in the dust storm, as demonstrated in laboratory experiments under simulated martian atmosphere conditions (*37*–*39*).

The decline in HCl, observed by ACS in MY35, is also indicative of an unexpected chemical sink for that species, which, in terms of the conventional gas-phase chemistry, is the stable reservoir of chlorine in the lower atmosphere of Mars (*40*). The transient nature of the observed HCl tells us that this does not constitute the whole picture and that we are missing an important chemical or physical loss process of chlorine. On Earth, laboratory studies have demonstrated the strong uptake coefficient of HCl on water ice surfaces at temperatures typical of those encountered on Mars (*41*, *42*). Water ice clouds are detected in our occultations during the whole dusty period, overlaying the dust, and, later, at lower altitudes, where we see HCl (*12*, *43*). In addition, surface frost is at a maximum at L_S = 270° (northern winter), when our northern HCl values are smaller. Heterogeneous HCl loss on surface ice would also be compatible with the shape of the profiles shown in Fig. 2 (A and C), showing decreasing mixing ratios near the surface.

Although our data do not permit a definitive determination of the source of HCl at this time, the coincidence of the GDS leads us to propose a novel surface-atmosphere interaction made plausible by terrestrial chemistry and recent laboratory studies. General circulation modeling is needed to constrain rates of HCl production and destruction and to probe possible sources of surface venting. The apparent link to dust activity will be examined during future dust events. Regardless of the HCl origin, it appears unlikely that the processes responsible for its production and destruction would not affect the rest of Mars' atmospheric chemistry. An impact on other gases is expected at altitudes above 30 km, where a greater fraction of chlorine is in the form of atomic Cl. The peak HCl concentrations on Mars ~1 to 4 ppbv are comparable to those in Earth's upper stratosphere and mesosphere (*44*). On Mars, the destructive ozone cycle, including odd oxygen, well known in Earth's stratosphere (*45*), would be ~20 times more efficient than assumed with previous upper limits on HCl. On the other hand, the transient nature of the HCl enhancement detected by ACS suggests the existence of a strong and unexpected loss process of that species, likely heterogeneous and efficient in the lower atmosphere or at the surface of Mars. Such a pathway may be photochemical and related to the advection pattern of other gases, such as H_2O, or to the absorption by dust itself (*46*). Our discovery suggests that the martian photochemistry should be revised, considering reactions with atmospheric dust or surface outgassing.

MATERIALS AND METHODS

The ACS instrument is a collection of three spectrometers operating in nadir and SO mode. The work presented here uses the ACS mid-infrared (ACS MIR) channel, which is a cross-dispersion echelle spectrometer. Solar light is dispersed by an echelle grating to measure the spectrum in the infrared range with high spectral resolving power ($\lambda/\Delta\lambda \sim 30{,}000$). Overlapping diffraction orders are then separated by a steerable secondary diffraction grating, the position of which determines the instantaneous spectral range (*7*). In this study, we use secondary grating positions 11 and 12, which provide spectral ranges of 2678 to 2948 cm^{-1} and 2917 to 3235 cm^{-1}, respectively, and divided into 16 to 20 diffraction orders. The diffraction orders related to the fundamental rotational band of HCl are shown in fig. S1, along with the contributions to transmission spectra by the absorption of CO_2, H_2O, HDO, and HCl. The partial overlap of the instantaneous spectral range in positions 11 and 12 permits measuring diffraction orders 173 to 175 in both positions. Figure S2 shows fits to HCl lines from both grating positions, in orders not presented in Fig. 1.

An ACS MIR detector image is a two-dimensional array of measured intensities. The *x* axis corresponds to wave number calibration, and the *y* axis corresponds to both the diffraction order and the tangent height of the instantaneous field of view (IFOV) (*7*). The appearance of a frame is several brightness stripes approximately 20 pixels wide, each one corresponding to a diffraction order in the mid-infrared (*14*). The IFOV covers 1 to 4 km, and each row provides a unique spectrum, separated by ~0.1 km.

Processing of the detector images was carried out at the Space Research Institute of the Russian Academy of Sciences (IKI RAS). A set of corrections is applied to each data frame that includes masking hot pixels, accounting for a subpixel drift in position caused by the instrument's thermal state, and an orthorectification. A dark image (I_{dark}) accounting for dark current and thermal drift is computed from the observations made when the sun is fully obscured. A solar reference image (I_{sun}) is computed by stacking observations made at tangent heights from 80 to ~250 km. For the spectral range provided by secondary grating positions 11 and 12, 80 km is sufficiently high to be free of gaseous absorption. The transmission at each altitude z is computed from the observations $I(z)$ as $(I(z) - I_{dark})/(I_{sun} - I_{dark})$. Additional details can be found in (*12*–*14*, *47*).

In ACS MIR, there is an effect, possibly caused by an optical component being damaged during launch, that results in the image of gaseous absorption lines to appear doubled. Rows for analysis are chosen by identifying the edge of the detector slit closest to the center of the solar disk, where this effect is minimized (a small "shoulder" is visible in spectra shown in fig. S2) (*10*, *13*, *14*). An instrument line shape can be modeled that accounts for this feature, and we have shown that it can be used to accurately retrieve trace gas abundances by validating results against those obtained from simultaneous observations made by the near-infrared (NIR) channel of ACS (*9*, *10*, *12*, *13*). Wave number calibration is performed for each row in two steps: first, by comparing the solar reference spectra to that measured by the Atmospheric Chemistry Experiment Fourier Transform Spectrometer (ACE-FTS) (*48*), and then, by comparing strong gas absorption lines, when available (*13*). Lastly, spectra are normalized using an alpha hull method (*49*).

Spectral fitting was performed using the Jet Propulsion Laboratory Gas Fitting Software suite (GGG or GFIT) (*50*–*52*). The atmosphere is modeled as homogeneous layers of 1-km thickness, and the optical path through each layer along the LOS is computed. For each fitting interval and for each spectrum, a forward model is computed using the instrument line shape described above and a Voigt line shape that depends on temperature and pressure and broadening parameters taken from the 2016 version of HITRAN line list (*53*). Vertical profiles of temperature and pressure were retrieved from CO_2 absorption features in simultaneous observations made by ACS NIR (*12*). The line depths are related to a gas' mixing ratio through the Beer-Lambert law, which depends on the line strength, taken from HITRAN 2016, the line shape, the temperature, and pressure of the atmosphere, and the optical path length. Vertical profiles of trace gas volume mixing ratios (VMRs) are estimated by inverting a matrix of LOS column abundances with a matrix of atmospheric layer contributions along the optical path. Uncertainties are computed from the Jacobian matrix of partial derivatives.

ACS results have been confirmed by two other analysis streams developed at the IKI and the Laboratoire Atmosphères, Milieux, Observations Spatiales (LATMOS) in support of the Mars Express Spectroscopy for Investigation of Characteristics of the Atmosphere of Mars instrument (*31*, *54*). The IKI code uses a Levenberg-Marquardt iterative approach to find the best solution for the gaseous composition of a model atmosphere, followed by applying Tikhonov regularization of the profile. This code has been adapted and used with ACS MIR (*9*) and ACS NIR (*12*) data. The LATMOS code uses a Levenberg-Marquardt regression scheme applied to transmittance spectra to infer the LOS integrated quantities of gases (*47*). The VMR is obtained by rationing the simultaneous observations of the targeted species (HCl in that case) with that of CO_2 calculated from fitting its 628 isotope *Q* branch in diffraction order 178. Derived gaseous vertical profiles are subsequently smoothed by convolving with a 1-km σ Gaussian kernel.

Detection limits have been estimated by measuring the noise of each spectrum and then performing spectral fitting with fixed quantities of HCl until modeled lines become prominent enough to cross a threshold value. The noise is measured by computing the difference between a spectrum and a smoothed spectrum. A smoothing window sufficiently wide to capture the variability of the signal caused by both random noise and larger systematic features is used, resulting in an SD of the noise that is consistent with that of the residuals of good spectral fits. A modest 2 SD threshold from a mean spectrum baseline value was used. The mean values, 1 and 2 SD thresholds, best-fit lines, and modeled spectra are shown in fig. S5 (A and B) for diffraction orders 174 and 175. The mean detection limit for these two orders, common to grating positions 11 and 12, is used to compute vertical profiles of detection limits, a selection of which are shown in fig. S5C. This method results in larger, more modest detection limits, appropriate for a gas that is now known to be present, than using the retrieval uncertainties. It is also more robust, as a best-fit line can occasionally suggest a negative gas value, which results in larger oscillation in a vertical profile of retrieval uncertainties. In total, 643 occultations have been analyzed in Fig. 3.

NOMAD is a set of spectrometers operating in the spectral ranges between 0.2 and 4.3 μm consisting of three channels. HCl has been observed with the SO channel, which uses an echelle grating used in combination with an acousto-optic tunable filter (AOTF) that selects the diffraction orders to be recorded (*8*, *55*). The diffraction order can be changed instantaneously by altering the frequency applied to the AOTF, and so, the SO channel is able to measure any

five or six selected diffraction orders per second within the entire spectral range of the channel. The illuminated rows on the detector are split into four individual bins, and a spectrum is recorded for each bin in every diffraction order from the top of the atmosphere (~200 km) to near the surface. Wave number calibration uses gaseous absorption lines, and a correction is applied to account for pixel nonlinearities.

For this work, SO channel data measured between April 2018 and February 2020, spanning both hemispheres, were analyzed. HCl features should be observed in several orders (125 to 130), and orders 129 (2889 to 2921 cm^{-1}) and 130 (2920 to 2943 cm^{-1}), which have been regularly observed, have been used to detect HCl. These datasets represent in total 264 observations in which 36 are positive detections. A positive detection is a 5-σ retrieved VMR for which the weighted average of the bins is greater than 0.3 ppb at more than two tangent heights (σ is the SD of the mean of retrievals from the four bins).

The HCl mixing ratio is retrieved by fitting the entire spectral range of either order 129 or 130. The temperature, pressure, and CO_2 VMR are taken from the values predicted by the GEM-Mars model (*56*) for each altitude, taking into account the GDS (*17*). Computed spectra are convolved with an instrument line shape, and the forward model accounts for the effects of the AOTF and the grating. Retrievals are performed using an optimal-estimation approach and line-by-line radiative transfer code (ASIMUT) developed for planetary atmospheres (*57*). Retrievals are performed independently at each tangential altitude (*11*). Figure S3 shows examples of bin-averaged spectra and best-fit lines for orders 129 and 130 featuring HCl absorption lines.

SUPPLEMENTARY MATERIALS

Supplementary material for this article is available at http://advances.sciencemag.org/cgi/content/full/7/7/eabe4386/DC1

REFERENCES AND NOTES

1. W. R. Simpson, S. S. Brown, A. Saiz-Lopez, J. A. Thornton, R. von Glasow, Tropospheric halogen chemistry: Sources, cycling, and impacts. *Chem. Rev.* **115**, 4035–4062 (2015).
2. Y. L. Yung, W. B. Demore, Photochemistry of the stratosphere of Venus: Implications for atmospheric evolution. *Icarus* **51**, 199–247 (1982).
3. A.-S. Wong, S. K. Atreya, T. Encrenaz, Chemical markers of possible hot spots on Mars. *J. Geophys. Res.* **108**, 5026 (2003).
4. P. Hartogh, C. Jarchow, E. Lellouch, M. de Val-Borro, M. Rengel, R. Moreno, A. S. Medvedev, H. Sagawa, B. M. Swinyard, T. Cavalié, D. C. Lis, M. I. Błęcka, M. Banaszkiewicz, D. Bockelée-Morvan, J. Crovisier, T. Encrenaz, M. Küppers, L.-M. Lara, S. Szutowicz, B. Vandenbussche, F. Bensch, E. A. Bergin, F. Billebaud, N. Biver, G. A. Blake, J. A. D. L. Blommaert, J. Cernicharo, L. Decin, P. Encrenaz, H. Feuchtgruber, T. Fulton, T. de Graauw, E. Jehin, M. Kidger, R. Lorente, D. A. Naylor, G. Portyankina, M. Sánchez-Portal, R. Schieder, S. Sidher, N. Thomas, E. Verdugo, C. Waelkens, N. Whyborn, D. Teyssier, F. Helmich, P. Roelfsema, J. Stutzki, H. G. LeDuc, J. A. Stern, Herschel/HIFI observations of Mars: First detection of O_2 at submillimetre wavelengths and upper limits on HCl and H_2O_2. *Astron. Astrophys.* **521**, L49 (2010).
5. G. L. Villanueva, M. J. Mumma, R. E. Novak, Y. L. Radeva, H. U. Käufl, A. Smette, A. Tokunaga, A. Khayat, T. Encrenaz, P. Hartogh, A sensitive search for organics (CH_4, CH_3OH, H_2CO, C_2H_6, C_2H_2, C_2H_4), hydroperoxyl (HO_2), nitrogen compounds (N_2O, NH_3, HCN) and chlorine species (HCl, CH_3Cl) on Mars using ground-based high-resolution infrared spectroscopy. *Icarus* **223**, 11–27 (2013).
6. J. Vago, O. Witasse, H. Svedhem, P. Baglioni, A. Haldemann, G. Gianfiglio, T. Blancquaert, D. McCoy, R. de Groot, ESA ExoMars program: The next step in exploring Mars. *Sol. Syst. Res.* **49**, 518–528 (2015).
7. O. Korablev, F. Montmessin, A. Trokhimovskiy, A. A. Fedorova, A. V. Shakun, A. V. Grigoriev, B. E. Moshkin, N. I. Ignatiev, F. Forget, F. Lefèvre, K. Anufreychik, I. Dzuban, Y. S. Ivanov, Y. K. Kalinnikov, T. O. Kozlova, A. Kungurov, V. Makarov, F. Martynovich, I. Maslov, D. Merzlyakov, P. P. Moiseev, Y. Nikolskiy, A. Patrakeev, D. Patsaev, A. Santos-Skripko, O. Sazonov, N. Semena, A. Semenov, V. Shashkin, A. Sidorov, A. V. Stepanov, I. Stupin, D. Timonin, A. Y. Titov, A. Viktorov, A. Zharkov, F. Altieri, G. Arnold, D. A. Belyaev, J. L. Bertaux, D. S. Betsis, N. Duxbury, T. Encrenaz, T. Fouchet, J.-C. Gérard, D. Grassi, S. Guerlet, P. Hartogh, Y. Kasaba, I. Khatuntsev, V. A. Krasnopolsky, R. O. Kuzmin, E. Lellouch, M. A. Lopez-Valverde, M. Luginin, A. Määttänen, E. Marcq, J. Martin Torres, A. S. Medvedev, E. Millour, K. S. Olsen, M. R. Patel, C. Quantin-Nataf, A. V. Rodin, V. I. Shematovich, I. Thomas, N. Thomas, L. Vazquez, M. Vincendon, V. Wilquet, C. F. Wilson, L. V. Zasova, L. M. Zelenyi, M. P. Zorzano, The Atmospheric Chemistry Suite (ACS) of three spectrometers for the ExoMars 2016 Trace gas orbiter. *Space Sci. Rev.* **214**, 7 (2018).
8. A. C. Vandaele, J.-J. Lopez-Moreno, M. R. Patel, G. Bellucci, F. Daerden, B. Ristic, S. Robert, I. R. Thomas, V. Wilquet, M. Allen, G. Alonso-Rodrigo, F. Altieri, S. Aoki, D. Bolsée, T. Clancy, E. Cloutis, C. Depiesse, R. Drummond, A. Fedorova, V. Formisano, B. Funke, F. González-Galindo, A. Geminale, J.-C. Gérard, M. Giuranna, L. Hetey, N. Ignatiev, J. Kaminski, O. Karatekin, Y. Kasaba, M. Leese, F. Lefèvre, S. R. Lewis, M. López-Puertas, M. López-Valverde, A. Mahieux, J. Mason, J. McConnell, M. Mumma, L. Neary, E. Neefs, E. Renotte, J. Rodriguez-Gomez, G. Sindoni, M. Smith, A. Stiepen, A. Trokhimovsky, J. V. Auwera, G. Villanueva, S. Viscardy, J. Whiteway, Y. Willame, M. Wolff, NOMAD, an integrated suite of three spectrometers for the ExoMars trace gas mission: Technical description, science objectives and expected performance. *Space Sci. Rev.* **214**, 80 (2018).
9. A. C. Vandaele, O. Korablev, F. Daerden, S. Aoki, I. R. Thomas, F. Altieri, M. López-Valverde, G. Villanueva, G. Liuzzi, M. D. Smith, J. T. Erwin, L. Trompet, A. A. Fedorova, F. Montmessin, A. Trokhimovskiy, D. A. Belyaev, N. I. Ignatiev, M. Luginin, K. S. Olsen, L. Baggio, J. Alday, J.-L. Bertaux, D. Betsis, D. Bolsée, R. T. Clancy, E. Cloutis, C. Depiesse, B. Funke, M. Garcia-Comas, J.-C. Gérard, M. Giuranna, F. Gonzalez-Galindo, A. V. Grigoriev, Y. S. Ivanov, J. Kaminski, O. Karatekin, F. Lefèvre, S. Lewis, M. López-Puertas, A. Mahieux, I. Maslov, J. Mason, M. J. Mumma, L. Neary, E. Neefs, A. Patrakeev, D. Patsaev, B. Ristic, S. Robert, F. Schmidt, A. Shakun, N. A. Teanby, S. Viscardy, Y. Willame, J. Whiteway, V. Wilquet, M. J. Wolff, G. Bellucci, M. R. Patel, J.-J. López-Moreno, F. Forget, C. F. Wilson, H. Svedhem, J. L. Vago, D. Rodionov; NOMAD Science Team; ACS Science Team, Martian dust storm impact on atmospheric H_2O and D/H observed by ExoMars Trace Gas Orbiter. *Nature* **568**, 521–525 (2019).
10. J. Alday, C. F. Wilson, P. G. J. Irwin, K. S. Olsen, L. Baggio, F. Montmessin, A. Trokhimovskiy, O. Korablev, A. A. Fedorova, D. A. Belyaev, A. Grigoriev, A. Patrakeev, A. Shakun, Oxygen isotopic ratios in Martian water vapour observed by ACS MIR on board the ExoMars Trace Gas Orbiter. *Astron. Astrophys.* **630**, A91 (2019).
11. S. Aoki, A. C. Vandaele, F. Daerden, G. L. Villanueva, G. Liuzzi, I. R. Thomas, J. T. Erwin, L. Trompet, S. Robert, L. Neary, S. Viscardy, R. T. Clancy, M. D. Smith, M. A. Lopez-Valverde, B. Hill, B. Ristic, M. R. Patel, G. Bellucci, J.-J. Lopez-Moreno; NOMAD Team, Water vapor vertical profiles on mars in dust storms observed by TGO/NOMAD. *J. Geophys. Res.* **124**, 3482–3497 (2019).
12. A. A. Fedorova, F. Montmessin, O. Korablev, M. Luginin, A. Trokhimovskiy, D. A. Belyaev, N. I. Ignatiev, F. Lefèvre, J. Alday, P. G. J. Irwin, K. S. Olsen, J.-L. Bertaux, E. Millour, A. Määttänen, A. Shakun, A. V. Grigoriev, A. Patrakeev, S. Korsa, N. Kokonkov, L. Baggio, F. Forget, C. F. Wilson, Stormy water on Mars: The distribution and saturation of atmospheric water during the dusty season. *Science* **367**, 297–300 (2020).
13. K. S. Olsen, F. Lefèvre, F. Montmessin, L. Baggio, A. Fedorova, A. Trokhimovskiy, O. Korablev, J. Alday, C. F. Wilson, D. Belyaev, A. Patrakeev, A. Grigoriev, A. Shakun, The vertical structure of CO in the Martian atmosphere as observed by ACS on ExoMars TGO. *Nat. Geosci.* https://doi.org/10.1038/s41561-020-00678-w (2021).
14. A. Trokhimovskiy, V. Perevalov, O. Korablev, A. F. Fedorova, K. S. Olsen, J.-L. Bertaux, A. Patrakeev, A. Shakun, F. Montmessin, First observation of the magnetic dipole CO_2 main isotopologue absorption band at 3.3μm in the atmosphere of Mars by the ExoMars Trace Gas Orbiter ACS instrument. *Astron. Astrophys.* **639**, A142 (2020).
15. K. S. Olsen, F. Lefèvre, F. Montmessin, A. Trokhimovskiy, L. Baggio, A. Fedorova, J. Alday, A. Lomakin, D. Belyaev, A. Patrakeev, A. Shakun, O. Korablev, First detection of ozone in the mid-infrared at Mars: Implications for methane detection. *Astron. Astrophys.* **639**, A141 (2020).
16. L. Montabone, A. Spiga, D. M. Kass, A. Kleinböhl, F. Forget, E. Millour, Martian year 34 column dust climatology from Mars climate sounder observations: Reconstructed maps and model simulations. *J. Geophys. Res.* **125**, e2019JE006111 (2020).
17. L. Neary, F. Daerden, S. Aoki, J. Whiteway, R. T. Clancy, M. Smith, S. Viscardy, J. T. Erwin, I. R. Thomas, G. Villanueva, G. Liuzzi, M. Crismani, M. Wolff, S. R. Lewis, J. A. Holmes, M. R. Patel, M. Giuranna, C. Depiesse, A. Piccialli, S. Robert, L. Trompet, Y. Willame, B. Ristic, A. C. Vandaele, Explanation for the increase in high altitude water on Mars observed by NOMAD during the 2018 global dust storm. *Geophys. Res. Lett.* **47**, e84354 (2020).
18. D. C. Catling, M. W. Claire, K. J. Zahnle, R. C. Quinn, B. C. Clark, M. H. Hecht, S. Kounaves, Atmospheric origins of perchlorate on Mars and in the Atacama. *J. Geophys. Res.* **115**, E00E11 (2010).
19. A. S. Khayat, G. L. Villanueva, M. J. Mumma, A. T. Tokunaga, A search for SO2, H2S and SO above Tharsis and Syrtis volcanic districts on Mars using ground-based high-resolution submillimeter spectroscopy. *Icarus* **253**, 130–141 (2015).

20. D. Giardini, P. Lognonné, W. B. Banerdt, W. T. Pike, U. Christensen, S. Ceylan, J. F. Clinton, M. van Driel, S. C. Stähler, M. Böse, R. F. Garcia, A. Khan, M. Panning, C. Perrin, D. Banfield, E. Beucler, C. Charalambous, F. Euchner, A. Horleston, A. Jacob, T. Kawamura, S. Kedar, G. Mainsant, J.-R. Scholz, S. E. Smrekar, A. Spiga, C. Agard, D. Antonangeli, S. Barkaoui, E. Barrett, P. Combes, V. Conejero, I. Daubar, M. Drilleau, C. Ferrier, T. Gabsi, T. Gudkova, K. Hurst, F. Karakostas, S. King, M. Knapmeyer, B. Knapmeyer-Endrun, R. Llorca-Cejudo, A. Lucas, L. Luno, L. Margerin, J. B. McClean, D. Mimoun, N. Murdoch, F. Nimmo, M. Nonon, C. Pardo, A. Rivoldini, J. A. R. Manfredi, H. Samuel, M. Schimmel, A. E. Stott, E. Stutzmann, N. Teanby, T. Warren, R. C. Weber, M. Wieczorek, C. Yana, The seismicity of Mars. *Nat. Geosci.* **13**, 205–212 (2020).
21. T. E. Graedel, W. C. Keene, Tropospheric budget of reactive chlorine. *Global Biogeochem. Cycles* **9**, 47–77 (1995).
22. J. M. Keller, W. V. Boynton, S. Karunatillake, V. R. Baker, J. M. Dohm, L. G. Evans, M. J. Finch, B. C. Hahn, D. K. Hamara, D. M. Janes, K. E. Kerry, H. E. Newsom, R. C. Reedy, A. L. Sprague, S. W. Squyres, R. D. Starr, G. J. T. R. M. S. Williams, Equatorial and midlatitude distribution of chlorine measured by Mars Odyssey GRS. *J. Geophys. Res.* **111**, E03S08 (2006).
23. J. A. Berger, M. E. Schmidt, R. Gellert, J. L. Campbell, P. L. King, R. L. Flemming, D. W. Ming, B. C. Clark, I. Pradler, S. J. V. Vanbommel, M. E. Minitti, A. G. Fairén, N. I. Boyd, L. M. Thompson, G. M. Perrett, B. E. Elliott, E. Desouza, A global mars dust composition refined by the alpha-particle X-ray spectrometer in gale crater. *Geophys. Res. Lett.* **43**, 67–75 (2016).
24. J. C. Bridges, M. M. Grady, A halite-siderite-anhydrite-chlorapatite assemblage in Nakhla: Mineralogical evidence for evaporites on Mars. *Meteor. Planet. Sci.* **34**, 407–415 (1999).
25. T. D. Glotch, J. L. Bandfield, M. J. Wolff, J. A. Arnold, C. Che, Constraints on the composition and particle size of chloride salt-bearing deposits on Mars. *Geophys. Res. Lett.* **121**, 454–471 (2016).
26. M. H. Hecht, S. P. Kounaves, R. C. Quinn, S. J. West, S. M. M. Young, D. W. Ming, D. C. Catling, B. C. Clark, W. V. Boynton, J. Hoffman, L. P. DeFlores, K. Gospodinova, J. Kapit, P. H. Smith, Detection of perchlorate and the soluble chemistry of martian soil at the phoenix lander site. *Science* **325**, 64–67 (2009).
27. D. P. Glavin, C. Freissinet, K. E. Miller, J. L. Eigenbrode, A. E. Brunner, A. Buch, B. Sutter, P. D. Archer, S. K. Atreya, W. B. Brinckerhoff, M. Cabane, P. Coll, P. G. Conrad, D. Coscia, J. P. Dworkin, H. B. Franz, J. P. Grotzinger, L. A. Leshin, M. G. Martin, C. McKay, D. W. Ming, R. Navarro-González, A. Pavlov, A. Steele, R. E. Summons, C. Szopa, S. Teinturier, P. R. Mahaffy, Evidence for perchlorates and the origin of chlorinated hydrocarbons detected by SAM at the Rocknest aeolian deposit in Gale Crater. *J. Geophys. Res.* **118**, 1955–1973 (2013).
28. B. C. Clark, S. P. Kounaves, Evidence for the distribution of perchlorates on Mars. *Int. J. Astrobiol.* **15**, 311–318 (2016).
29. D. L. Santiago-Materese, L. T. Iraci, M. E. Clapham, P. Y. Chuang, Chlorine-containing salts as water ice nucleating particles on Mars. *Icarus* **303**, 280–287 (2018).
30. I. J. George, J. P. D. Abbatt, Heterogeneous oxidation of atmospheric aerosol particles by gas-phase radicals. *Nat. Chem.* **2**, 713–722 (2010).
31. A. Fedorova, J.-L. Bertaux, D. Betsis, F. Montmessin, O. Korablev, L. Maltagliati, J. Clarke, Water vapor in the middle atmosphere of Mars during the 2007 global dust storm. *Icarus.* **300**, 440–457 (2018).
32. M. L. Smith, M. W. Claire, D. C. Catling, K. J. Zahnle, The formation of sulfate, nitrate and perchlorate salts in the martian atmosphere. *Icarus* **231**, 51–64 (2014).
33. E. H. Wilson, S. K. Atreya, R. I. Kaiser, P. R. Mahaffy, Perchlorate formation on Mars through surface radiolysis-initiated atmospheric chemistry: A potential mechanism. *J. Geophys. Res.* **121**, 1472 (2016).
34. J. C. Stern, B. Sutter, W. A. Jackson, R. Navarro-González, C. P. McKay, D. W. Ming, P. D. Archer, P. R. Mahaffy, The nitrate/(per)chlorate relationship on Mars. *Geophys. Res. Lett.* **44**, 2643–2651 (2017).
35. D. C. Catling, M. L. Smith, M. W. Claire, K. J. Zahnle, paper presented at the EPSC, London, UK, 2013.
36. B. L. Carrier, S. P. Kounaves, The origins of perchlorate in the Martian soil. *Geophys. Res. Lett.* **42**, 3739–3745 (2015).
37. B. Rao, S. Mohan, A. Neuber, W. A. Jackson, Production of perchlorate by laboratory simulated lightning process. *Water Air Soil Pollut.* **223**, 275–287 (2012).
38. P. U. Martínez-Pabello, R. Navarro-González, X. Walls, T. Pi-Puig, J. L. González-Chávez, J. G. de la Rosa, P. Molina, O. Zamora, Production of nitrates and perchlorates by laser ablation of sodium chloride in simulated Martian atmospheres. Implications for their formation by electric discharges in dust devils. *Life Sci. Space Res.* **22**, 125–136 (2019).
39. A. Wang, Y. Yan, B. L. Jolliff, S. M. McLennan, K. Wang, E. Shi, W. M. Farrell, Chlorine release from common chlorides by martian dust activity. *J. Geophys. Res.* **125**, e2019JE006283 (2020).
40. F. Lefèvre, V. Krasnopolsky, *The Atmosphere and Climate of Mars*, R. M. Haberle, R. T. Clancy, F. Forget, M. D. Smith, R. W. Zurek, Eds. (Cambridge Planetary Science, Cambridge University Press, 2017), pp. 405–432.
41. J. B. Burkholder, S. P. Sander, J. P. D. Abbatt, J. R. Barker, R. E. Huie, C. E. Kolb, M. J. Kurylo, V. L. Orkin, D. M. Wilmouth, P. H. Wine, *Chemical Kinetics and Photochemical Data for Use in Atmospheric Studies: Evaluation Number 18*, (Technical Report, Jet Propulsion Laboratory, NASA, 2015).
42. M. Kippenberger, G. Schuster, J. Lelieveld, J. N. Crowley, Trapping of HCl and oxidised organic trace gases in growing ice at temperatures relevant to cirrus clouds. *Atmos. Chem. Phys.* **19**, 11939–11951 (2019).
43. G. Liuzzi, G. L. Villanueva, M. M. J. Crismani, M. D. Smith, M. J. Mumma, F. Daerden, S. Aoki, A. C. Vandaele, R. T. Clancy, J. Erwin, I. Thomas, B. Ristic, J.-J. Lopez-Moreno, G. Bellucci, M. R. Patel, Strong variability of Martian water ice clouds during dust storms revealed from ExoMars Trace Gas Orbiter/NOMAD. *J. Geophys. Res.* **125**, e2019JE006250 (2020).
44. L. Froidevaux, Y. B. Jiang, A. Lambert, N. J. Livesey, W. G. Read, J. W. Waters, R. A. Fuller, T. P. Marcy, P. J. Popp, R. S. Gao, D. W. Fahey, K. W. Jucks, R. A. Stachnik, G. C. Toon, L. E. Christensen, C. R. Webster, P. F. Bernath, C. D. Boone, K. A. Walker, H. C. Pumphrey, R. S. Harwood, G. L. Manney, M. J. Schwartz, W. H. Daffer, B. J. Drouin, R. E. Cofield, D. T. Cuddy, R. F. Jarnot, B. W. Knosp, V. S. Perun, W. V. Snyder, P. C. Stek, R. P. Thurstans, P. A. Wagner, Validation of aura microwave limb sounder HCl measurements. *J. Geophys. Res.* **113**, D15S25 (2008).
45. G. P. Brasseur, S. Solomon, *Aeronomy of the Middle Atmosphere: Chemistry and Physics of the Stratosphere and Mesosphere* (Atmospheric and Oceanographic Sciences Library, Springer Netherlands, ed. 3, 2005).
46. C. R. Webster, H. A. Michelsen, M. R. Gunson, J. J. Margitan, J. M. Russell, G. C. Toon, W. A. Traub, Response of lower stratospheric HCl/Cl_y to volcanic aerosol: Observations from aircraft, balloon, space shuttle, and satellite instruments. *J. Geophys. Res.* **105**, 11711–11719 (2000).
47. O. Korablev, A. C. Vandaele, F. Montmessin, A. A. Fedorova, A. Trokhimovskiy, F. Forget, F. Lefèvre, F. Daerden, I. R. Thomas, L. Trompet, J. T. Erwin, S. Aoki, S. Robert, L. Neary, S. Viscardy, A. Grigoriev, N. Ignatiev, A. Shakun, A. Patrakeev, D. Belyaev, J.-L. Bertaux, K. S. Olsen, L. Baggio, J. Alday, Y. S. Ivanov, B. Ristic, J. Mason, Y. Willame, C. Depiesse, L. Hetey, S. Berkenbosch, R. Clairquin, C. Queirolo, B. Beeckman, E. Neefs, M. R. Patel, G. Bellucci, J.-J. López-Moreno, C. F. Wilson, G. Etiope, L. Zelenyi, H. Svedhem, J. L. Vago; The ACS and NOMAD Science Teams, No detection of methane on Mars from early ExoMars Trace Gas Orbiter observations. *Nature* **568**, 517–520 (2019).
48. F. Hase, L. Wallace, S. D. McLeod, J. J. Harrison, P. F. Bernath, The ACE-FTS atlas of the infrared solar spectrum. *J. Quant. Spectrosc. Radiat. Transfer.* **111**, 521–528 (2010).
49. X. Xu, J. Cisewski-Kehe, A. B. Davis, D. A. Fischer, J. M. Brewer, Modeling the Echelle spectra continuum with alpha shapes and local regression fitting. *Astron. J.* **157**, 243 (2019).
50. F. W. Irion, M. R. Gunson, G. C. Toon, A. Y. Chang, A. Eldering, E. Mahieu, G. L. Manney, H. A. Michelsen, E. J. Moyer, M. J. Newchurch, G. B. Osterman, C. P. Rinsland, R. J. Salawitch, B. Sen, Y. L. Yung, R. Zander, Atmospheric Trace Molecule Spectroscopy (ATMOS) experiment version 3 data retrievals. *Appl. Optics* **41**, 6968–6979 (2002).
51. B. Sen, G. C. Toon, J.-F. Blavier, E. L. Fleming, C. H. Jackman, Balloon-borne observations of midlatitude fluorine abundance. *J. Geophys. Res.* **101**, 9045–9054 (1996).
52. D. Wunch, G. C. Toon, J. L. Blavier, R. A. Washenfelder, J. Notholt, B. J. Connor, D. W. T. Griffith, V. Sherlock, P. O. Wennberg, The total carbon column observing network. *Philos. Trans. R. Soc. A Math. Phys. Eng. Sci.* **369**, 2087–2112 (2011).
53. I. E. Gordon, L. S. Rothman, C. Hill, R. V. Kochanov, Y. Tan, P. F. Bernath, M. Birk, V. Boudon, A. Campargue, K. V. Chance, B. J. Drouin, J.-M. Flaud, R. R. Gamache, J. T. Hodges, D. Jacquemart, V. I. Perevalov, A. Perrin, K. P. Shine, M.-A. H. Smith, J. Tennyson, G. C. Toon, H. Tran, V. G. Tyuterev, A. Barbe, A. G. Császár, V. M. Devi, T. Furtenbacher, J. J. Harrison, J.-M. Hartmann, A. Jolly, T. J. Johnson, T. Karman, I. Kleiner, A. A. Kyuberis, J. Loos, O. M. Lyulin, S. T. Massie, S. N. Mikhailenko, N. Moazzen-Ahmadi, H. S. P. Müller, O. V. Naumenko, A. V. Nikitin, O. L. Polyansky, M. Rey, M. Rotger, S. W. Sharpe, K. Sung, E. Starikova, S. A. Tashkun, J. V. Auwera, G. Wagner, J. Wilzewski, P. Wcislo, S. Yu, E. J. Zak, The HITRAN2016 molecular spectroscopic database. *J. Quant. Spectrosc. Radiat. Transfer.* **203**, 3–69 (2017).
54. A. A. Fedorova, O. I. Korablev, J.-L. Bertaux, A. V. Rodin, F. Montmessin, D. A. Belyaev, A. Reberac, Solar infrared occultation observations by SPICAM experiment on Mars-Express: Simultaneous measurements of the vertical distributions of H_2O, CO_2 and aerosol. *Icarus* **200**, 96–117 (2009).
55. E. Neefs, A. C. Vandaele, R. Drummond, I. R. Thomas, S. Berkenbosch, R. Clairquin, S. Delanoye, B. Ristic, J. Maes, S. Bonnewijn, G. Pieck, E. Equeter, C. Depiesse, F. Daerden, E. V. Ransbeeck, D. Nevejans, J. Rodriguez-Gómez, J.-J. López-Moreno, R. Sanz, R. Morales, G. P. Candini, M. C. Pastor-Morales, B. A. del Moral, J.-M. Jeronimo-Zafra, J. M. Gómez-López, G. Alonso-Rodrigo, I. Pérez-Grande, J. Cubas, A. M. Gomez-Sanjuan, F. Navarro-Medina, T. Thibert, M. R. Patel, G. Bellucci, L. De Vos, S. Lesschaeve, N. V. Vooren, W. Moelans, L. Aballea, S. Glorieux, A. Baeke, D. Kendall, J. De Neef, A. Soenen, P.-Y. Puech, J. Ward, J.-F. Jamoye, D. Diez, A. Vicario-Arroyo, M. Jankowski, NOMAD spectrometer on the ExoMars trace gas orbiter mission: Part 1—Design, manufacturing and testing of the infrared channels. *Appl. Optics* **54**, 8494–8520 (2015).
56. F. Daerden, L. Neary, S. Viscardy, A. García Muñoz, R. T. Clancy, M. D. Smith, T. Encrenaz, A. Fedorova, Mars atmospheric chemistry simulations with the GEM-Mars general circulation model. *Icarus* **326**, 197–224 (2019).

57. A. C. Vandaele, M. D. Mazière, R. Drummond, A. Mahieux, E. Neefs, V. Wilquet, O. Korablev, A. Fedorova, D. Belyaev, F. Montmessin, J.-L. Bertaux, Composition of the Venus mesosphere measured by Solar Occultation at Infrared on board Venus Express. *J. Geophys. Res.* **113**, E00B23 (2008).

Acknowledgments: The ExoMars mission was jointly developed and operated by ESA and Roscosmos. The ACS experiment is led by the Space Research Institute (IKI) in Moscow, assisted by LATMOS in France. The NOMAD experiment is led by the Royal Belgian Institute for Space Aeronomy (IASB-BIRA), assisted by teams from Spain (IAA-CSIC), Italy (INAF-IAPS), and the United Kingdom (Open University). D. Catling (University of Washington, Seattle), J. Abbatt (University of Toronto), and F. Forget (LMD/CNRS) provided insightful feedback on this paper. **Funding:** The ACS project acknowledges funding by Roscosmos and CNES. The science operations of ACS are funded by Roscosmos and ESA. IKI affiliates acknowledge funding from the Russian Science Foundation (RSF-ANR 20-42-09035) (data analysis and interpretation). University of Oxford affiliates acknowledge funding from the UK Space Agency (ST/T002069/1 and ST/R001502/1), the Natural Sciences and Engineering Research Council of Canada (NSERC) (PDF-516895-2018), and CNES. LATMOS affiliates acknowledge funding from CNES and ANR (PRCI, CE31 AAPG2019-MCUBE project). The NOMAD Team acknowledges funding by the Belgian Science Policy Office (BELSPO), with the financial and contractual coordination by the ESA Prodex Office (PEA 4000103401 and 4000121493), by the Spanish MICINN through its Plan Nacional and by the European funds (grants PGC2018-101836-B-I00 and ESP2017-87143-R) (MINECO/FEDER), by the UK Space Agency (grants ST/R005761/1, ST/P001262/1, ST/R001405/1, and ST/S00145X/1), by the Italian Space Agency (grant 2018-2-HH.0. S), and by the Spanish Science Ministry Centro de Excelencia Severo Ochoa Program (grant SEV-2017-0709). S.A. acknowledges funding from the Belgian Fund for Scientific Research (FNRS). **Author contributions:** K.S.O. has first recognized the HCl signature in ACS spectra. O.K., K.S.O., F.L., and F.M. conceived the study and wrote the paper. A.T., assisted by L.B., Y.S.I., and A.P., prepared and calibrated the ACS dataset. K.S.O., with the help of F.M., A.A.F., A.T., and I.A., analyzed the ACS data, retrieved profiles, and upper limits. A.A.F., assisted by A.T., J.A., D.A.B., and N.I.I., retrieved supportive information. A.T., A.P., A.V.S., A.V.G., and G.L. have designed ACS observations. S.A. analyzed the NOMAD data. I.R.T. and J.T.E. calibrated the data and planned the observations, assisted by B.R. F.D. investigated the scientific relevance of the detection. A.C.V., M.P., G.B., and J.-J.L.-M. supervised the scientific observations of NOMAD. M.J.T. provided inputs on geochemical and heterogeneous chemistry pathways. **Competing interests:** The authors declare that they have no competing interests. **Data availability:** The datasets generated by the ACS and NOMAD instruments and analyzed during the current study are available in the ESA Planetary Science Archive repository (https://archives.esac.esa.int/psa). The datasets used directly in this study, including the data used for the figures are available at https://doi.org/10.5287/bodleian:aZnnj76MY. All data needed to evaluate the conclusions in the paper are present in the paper and/or the Supplementary Materials. Additional data related to this paper may be requested from the authors.

Submitted 21 August 2020
Accepted 28 December 2020
Published 10 February 2021
10.1126/sciadv.abe4386

Citation: O. Korablev, K. S. Olsen, A. Trokhimovskiy, F. Lefèvre, F. Montmessin, A. A. Fedorova, M. J. Toplis, J. Alday, D. A. Belyaev, A. Patrakeev, N. I. Ignatiev, A. V. Shakun, A. V. Grigoriev, L. Baggio, I. Abdenour, G. Lacombe, Y. S. Ivanov, S. Aoki, I. R. Thomas, F. Daerden, B. Ristic, J. T. Erwin, M. Patel, G. Bellucci, J.-J. Lopez-Moreno, A. C. Vandaele, Transient HCl in the atmosphere of Mars. *Sci. Adv.* **7**, eabe4386 (2021).